PERGAMON

International Journal of Solids and Structures 40 (2003) 5521–5538

INTERNATIONAL JOURNAL OF SOLIDS and STRUCTURES

www.elsevier.com/locate/ijsolstr

Mechanisms of stress transfer and interface integrity in carbon/epoxy composites under compression loading. Part II: Numerical approach

S. Goutianos [a,b,*], C. Galiotis [a,b,c], T. Peijs [a]

[a] *Department of Materials, Queen Mary University of London, Mile End Road, London E1 4NS, UK*

[b] *Institute of Chemical Engineering and High Temperature Chemical Processes, Foundation of Research and Technology—Hellas, P.O. Box 1414, Patras 265 00, Greece*

[c] *Department of Materials Science, School of Natural Sciences, University of Patras, Patras 265 04, Greece*

Received 10 June 2003; received in revised form 10 June 2003

Abstract

The finite element method is used to get an insight into the micromechanics of the compressive behaviour of carbon fibre composites. First the developed model is validated with existing experimental data and good agreement between predictions and experiments was found. Then the FE model is used to derive the complete stress field in the fibre and the matrix in the vicinity of a fibre fracture location. It was found that the perturbation of the stress field occurs mainly in the direction transverse to the fibre axis and this could explain the failure modes observed in composites tested in compression. Finally, a parametric study was performed on the effect of matrix modulus and matrix yield stress on the compressive fragmentation process.

Keywords: Compression; Carbon fibres; Interfacial shear stress; Composites

1. Introduction

Polymer composites possess excellent tensile properties due to the high tensile strength of the fibres. However, their compressive strength is often less than 60% of their respective tensile strength (Budiansky and Fleck, 1991). It is widely accepted, nowadays, that the observed composite inherent weakness in compression is related to a plastic microbuckling process (Argon, 1972; Budiansky, 1983; Jensen, 2002). In general, the compressive strength, σ_u^c, is given as a function of the initial fibre misalignment and the matrix or composite shear yield strength (Christensen and De Teresa, 1997; Fleck et al., 1995):

* Corresponding author. Address: Department of Materials, Queen Mary University of London, Mile End Road, London E1 4NS, UK. Tel.: +44-20-7882-7879; fax: +44-20-8981-9804.

E-mail address: s.goutianos@qmul.ac.uk (S. Goutianos).

0020-7683/$ - see front matter © 2003 Published by Elsevier Ltd.
doi:10.1016/S0020-7683(03)00340-8

$$\sigma_u^c = \frac{G_{LT}^c}{1 + \frac{\varphi_0}{\gamma_y^c}} \tag{1}$$

where G_{LT}^c is the composite shear modulus, φ_0 is the initial fibre misalignment and γ_y^c is the composite shear yield strain.

The predictions of Eq. (1) are close to the compressive strength values experimentally measured (Soutis and Curtis, 2000; Soutis et al., 2000), and significantly lower than Rosen's analysis (fibre buckling in an elastic matrix) (Rosen, 1965). It should be mentioned, however, that there is usually a large degree of uncertainty concerning the fibre misalignment (see Eq. (1)) in a composite. More importantly, these analyses fail short to capture the physics of the problem (Schapery, 1995). As a consequence, alternative theories have been developed, which consider the possibility of the failure being controlled by the compressive failure of the fibres. Kozey (1993) concluded that stress raisers have an important effect on carbon–fibre composites. He suggested the possibility of strain concentrations leading to compressive failure. This is well demonstrated in the work of Lankford (1995) who showed that a cluster of broken fibres forms a defect zone, which in turn leads to kink band formation. Moreover, he suggested that these initial fibre breaks would lie along parallel shear bands rather than normal to the reinforcement direction. Narayanan and Schadler (1999a) expanded Lankford's ideas and have used the Laser Raman Spectroscopy technique to study kink band initiation in carbon–epoxy composites. In agreement with Lankford's work, they suggested that once the damage zone, consisting of broken and/or crushed fibres, reaches a critical size, local instability causes microbuckling. Recently, Garland et al. (2001) developed a simple shear-lag model to calculate the stress state around broken fibres, which has been used to predict the formation of damage zones. Their work and its limitations are discussed in more detail in the following section.

Such theories, described above, could also explain i.e. the role of the interfacial properties in the compressive behaviour in contrast to the family of matrix shear strength and fibre misalignment-dominated theories (Lankford, 1995). For example Madhukar and Drzal (1992) have shown that by increasing the interfacial shear strength (ISS), while keeping the matrix yield strength and fibre orientation constant, compressive strength increases and at the same time the failure mode changes from delamination to microbuckling. Similar results were also reported by Lesko et al. (1994), who found significantly increased compressive strength values by increasing the ISS or the interfacial strain to failure.

From the above, it can be argued that the fundamental issues, of the compressive behaviour of fibrous composites still remain open. The problem of compressive failure is more complicated than is generally appreciated (Lankford, 1995) and appropriate models should include the role of fibre strength and its distribution, matrix properties, and interfacial properties. In a previous work (Goutianos et al., 2002a) the laser Raman spectroscopy technique was used to get an insight into the microstructural aspects of the compressive behaviour of carbon/epoxy composites. This was done by a comparative assessment of the stress transfer efficiency in tension and compression in single fibre discontinuous model geometries. The stress transfer mechanisms were completely described in the region around the fibre ends, however, this was not the case in the vicinity of a compressive fibre break since in this case the balance of forces argument (required to derive the interfacial shear stresses) breaks down (Goutianos et al., 2002a). Narayanan and Schadler (1999b) have employed the balance of forces argument to calculate the ISS in the case of a compressive fibre break, their reported ISS values were in excess of 150 MPa or even 300 MPa (Amer and Schadler, 1997) for fibre/matrix systems similar with the system examined here and in our previous work (Goutianos et al., 2002a). Since these values were unacceptably high, an attempt was made (Narayanan and Schadler, 1999b) to modify the balance of forces argument to account for the post-failure geometric configuration. Although the new ISS values were reduced these values were still too high and as stated by the same authors, a more rigorous analysis is needed to estimate accurately the interfacial shear stress in the

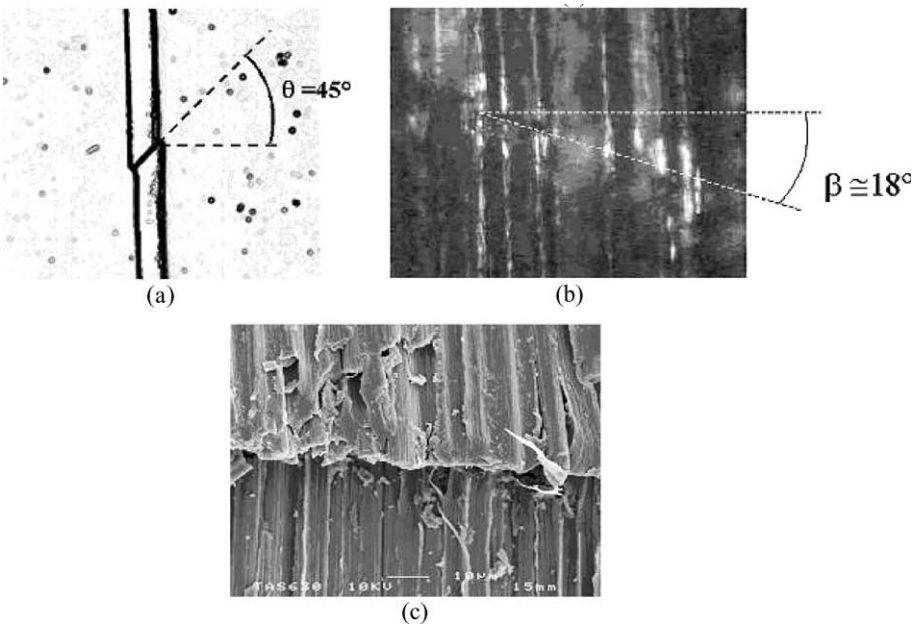

Fig. 1. (a) Micrograph of a typical compression induced shear fibre break, (b) micrograph of a fracture site showing fibres failed in shear at a well defined plane, (c) SEM picture showing again co-operative fibre shear failure in compression.

neighbourhood of a compressive fibre break. As a result in the current work, the finite element method is employed to study the complex stress field (in both the fibre and the matrix) generated by a compressive fibre break (shear failure).

Fig. 1(a) shows a micrograph of a typical compression induced shear fibre break, it can be easily seen that the broken ends slide past each other and therefore compressive stresses can be transmitted as the fibre fragments remain in contact (Goutianos et al., 2002a). The same failure mode can be also observed in multi-fibre model composites (Fig. 1(b) and (c)), that is the fibres have failed in shear at a certain (well defined) plane, whereas no fibre fractures were observed far from the fracture planes (Goutianos et al., 2002b). Fig. 1 clearly indicates the importance of understanding the stresses generated around a fibre break, which would probably enrich our knowledge concerning damage development in compression. In the current work only a single-carbon fibre embedded in an epoxy matrix will be considered at first instance, while the case of a planar array of fibres will be reported in a subsequent work.

2. FE model for fibre fracture in compression

Various analytical models (2D or 3D) have been developed over the past years (e.g. Nath et al., 1996; Van den Heuvel et al., 1998; Sirivedin et al., 2000) for the derivation of stresses in both the fibre and the matrix in single or multi-fibre composites. These analyses, however, are restricted in the case of tensile loading. In contrast, very little work has been reported in the literature concerning numerical modelling of the compressive behaviour of composites at micromechanical level. Usually the uniaxial composite is investigated using two or three-dimensional micromechanical models, which include a global (Hsu et al., 1999a,b) or local (Vogler et al., 2001; Byskov et al., 2002) imperfection by means of fibre misalignment. These global or local imperfections are required in order to initiate the kink band formation. Kink band initiation and growth are by a fibre microbuckling process. Fibre fracture is not considered in these analyses

since it is assumed that it might be a 'post-failure' event, that is the fibres may fail due to excessive buckling. To the best of our knowledge the compressive fragmentation process has not yet been investigated by means of a numerical or even more an analytical model mainly due to the complexity of the problem and lack of experimental data with the exception of the work of Garland et al. (2001), which has been already mentioned above. They have used a break-influence superposition technique (Sastry and Phoenix, 1993) based on a simple shear-lag model to study the development of compression damage zones. As almost every shear-lag model, their model presents some major drawbacks such as it assumes that the matrix only deforms in shear and its axial stiffness is ignored. More importantly the fibres are not allowed to deform in the transverse direction, which is not the case as can be seen in Fig. 1(a). As a result of this fibre shearing restriction, their predicted stress profiles are quite symmetric and similar to the tensile case, while according to the experimental results (Goutianos et al., 2002a) the fibre stress profiles are not symmetric along the fibre length. The same will be shown later in the following section by means of FE analysis. Furthermore, the assumption that the fibre stress is zero at the break point is not supported by the experimental data of Goutianos et al. (2002a). Finally, their key assumption that the peak stress concentration produced by an angled break (i.e. like the one shown in Fig. 1(a)) is the same as that of a straight break is questionable. However, despite these drawbacks, their work shows nicely how a damage zone of broken fibres could lead to kink band formation. Thus here we attempt to model the compressive behaviour of a (at first instance) single-carbon fibre embedded in an epoxy matrix by means of FEA, although this results in an intense computation compared to the technique used by Garland et al. (2001). This material system is identical to the system experimentally studied in previous works (Goutianos et al., 2002a,b).

2.1. Finite element details

2.1.1. The mesh

The single-fibre model composite was implemented in the ABAQUS finite element code. The I-DEAS pre-processor was used to generate the mesh of the microcomposite. Clearly the problem of the fibre fracture in compression (see Fig. 1(a)) is a three-dimensional problem. In this case, however, the complexity and size of the model significantly increase which is beyond the scope of the current work. Moreover, due to the shear-failure of the fibre, the problem cannot be considered as an axisymmetric one. Thus, we have chosen to model the fibre fracture problem as a plane stress problem. A schematic representation of the model is depicted in Fig. 2. Fibre fracture is assumed to occur in the centre of the model composite. The fibre is then divided in two fragments, which are fully bonded up to a certain applied strain level (equal to

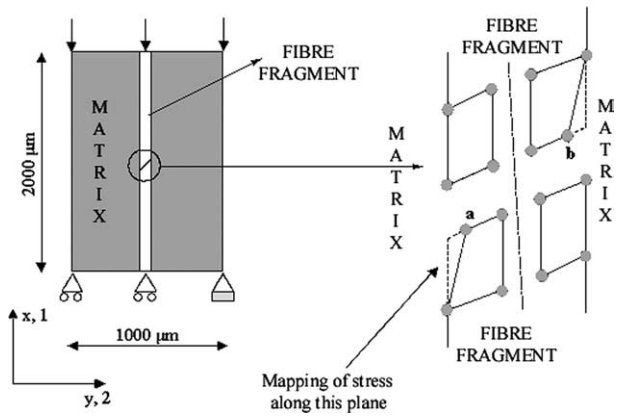

Fig. 2. Schematic representation of the FE model used.

the fibre failure strain experimentally determined in similar specimens (Goutianos et al., 2002a)). The angle between the fibre fragments is 45°, equal to the value observed in the experiments (see Fig. 1(a)). In the subsequent step of the analysis the coefficient of friction between the fibre fragments is reduced allowing in that way the fibre fragments to slide past each other. The fibre fragments (near the fracture site) are also fully bonded to the surrounding matrix using the TIED CONTACT option of ABAQUS. Due to the multi-contact nature of the model, bilinear four noded elements had to be used. The fibre close to the contact area (see Fig. 2) was modelled using incompatible modes elements in order to prevent shear locking or hourglass effects. At this point, it should be noted that as the fibre fragments slide past each other, bending of the fibre fragments occurs. Full integration elements were found to give poor results in this case due to shear locking, whereas reduced integration elements were sensitive to hourglass effects. Thus, the use of incompatible elements was necessary although this resulted in significant increase of the computational time. The fibre fragments far from the contact area (fibre fracture site) and the matrix material were modelled using full integration elements. Finally, in order to facilitate the multi-contact definition, node a and b belonging to the fibre fragments were slightly moved as it can be seen in Fig. 2. This kind of local imperfection results in stress discontinuities at applied strains even much lower than the strain level at which the fibre fragments are allowed to slide past each other. As it will be shown, however, in the results section this imperfection has minor effects in the overall analysis. Finally, it should be mentioned that the analysis performed was quasi-static, that is any dynamic effect from the fibre fracture is excluded. This is the case, however, also in the experimental work on the same material system (Goutianos et al., 2002a). Thus, comparison of the numerical predictions versus experiments is still valid.

The axial fibre stress is calculated at the right hand side of the fibre as it is shown in Fig. 2, whereas the interfacial shear and transverse stresses are calculated at the corresponding fibre/matrix interface.

2.1.2. Boundary conditions and applied loads

Through the analysis the nodes at $x = 0$ (see Fig. 2) are fixed in the x-direction, whereas the far bottom right matrix node is also constrained in the y-direction. A total strain of −0.8% with respect to the initial x-length of the model is applied at the nodes at $x = 2000$ μm. Up to an applied strain of −0.5% the fibre fragments are constrained to move relative to each other. Then, as it was mentioned above, at an applied strain of −0.55% (fibre failure strain in the microcomposite) the coefficient of friction between the fibre fragments is decreased allowing the fibre fragments to slide past each other.

2.1.3. Material properties

The fibre is modelled as an anisotropic continuum with linear elastic behaviour in both compression and tension. The fibre properties are listed in Table 1. Concerning the epoxy matrix, an elasto-plastic behaviour is assumed. Fig. 3 depicts the experimental stress–strain curve for the epoxy matrix, whereas its mechanical properties are given in Table 1. It should be mentioned here that in the results section, the effect of matrix

Table 1
Mechanical properties of fibre and resin

Mechanical parameters	M40-40B carbon fibre	Epoxy matrix
E_1 (GPa)	390	2
E_2 (GPa)	20	2
ν_{12} (–)	0.03	0.30
G_{12} (GPa)	12	0.77
G_{13} (GPa)	5	0.77
G_{23} (GPa)	12	0.77

E: Young's modulus, G: shear modulus, ν: Poisson's ratio, 1: longitudinal direction, 2: transverse direction, 3: out of plane direction.

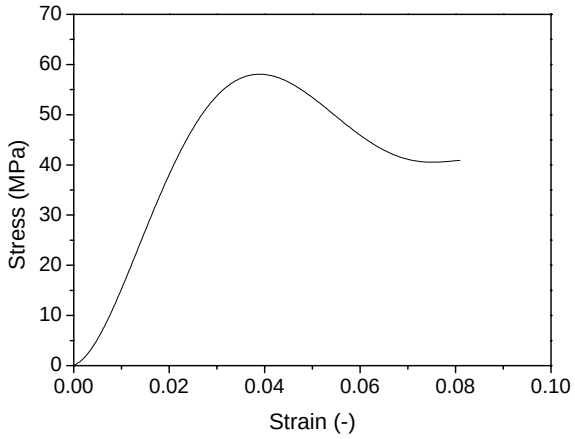

Fig. 3. Stress–strain curve for the epoxy matrix.

modulus and the effect of matrix yield stress on the stresses generated around the fibre fracture are investigated assuming an elastic–perfectly plastic behaviour for the epoxy matrix.

3. Results and discussion

3.1. Effect of fibre geometrical discontinuity on the stress field

As it was referred in the previous section a geometrical imperfection was introduced in the model definition in the area where the fibre break is introduced. In this section, the effect of this imperfection will be briefly investigated. Fig. 4 depicts the axial fibre stress (σ_{11}) at different applied strain levels (−0.3%, −0.4%, and −0.5%, respectively), which are lower than the applied strain at which the fibre break is introduced (−0.55%). As it can be seen the fibre stress is constant along the fibre length as expected. At $x = 1000$ μm, however, a fibre stress perturbation can be observed due to the initially introduced imperfection. The same

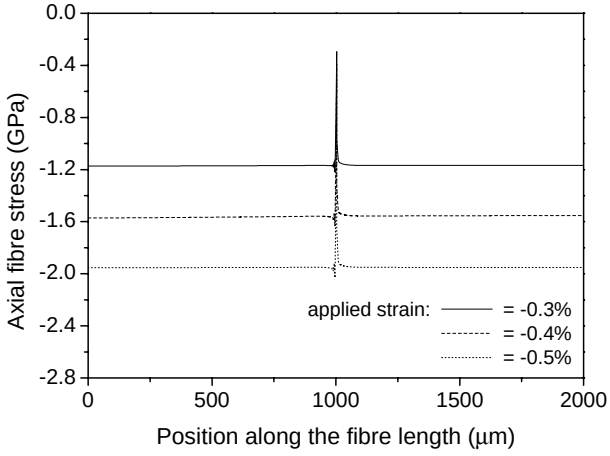

Fig. 4. Axial fibre stress of an embedded fibre ($L_f = 2$ mm) in an epoxy matrix, loaded at strain of −0.3%, −0.4%, and −0.5%, respectively.

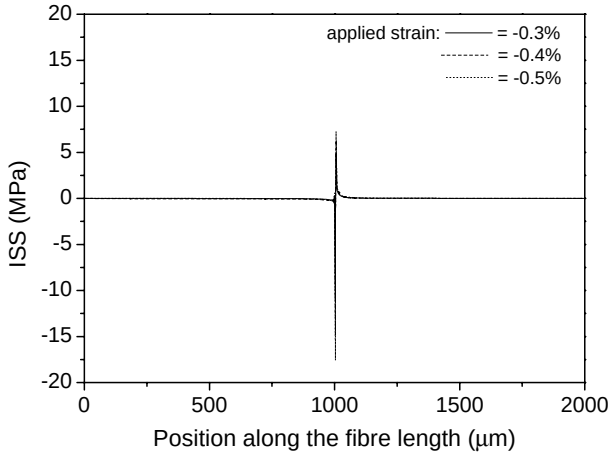

Fig. 5. Corresponding interfacial shear stresses of Fig. 4. The applied strains are −0.3%, −0.4%, and −0.5%, respectively.

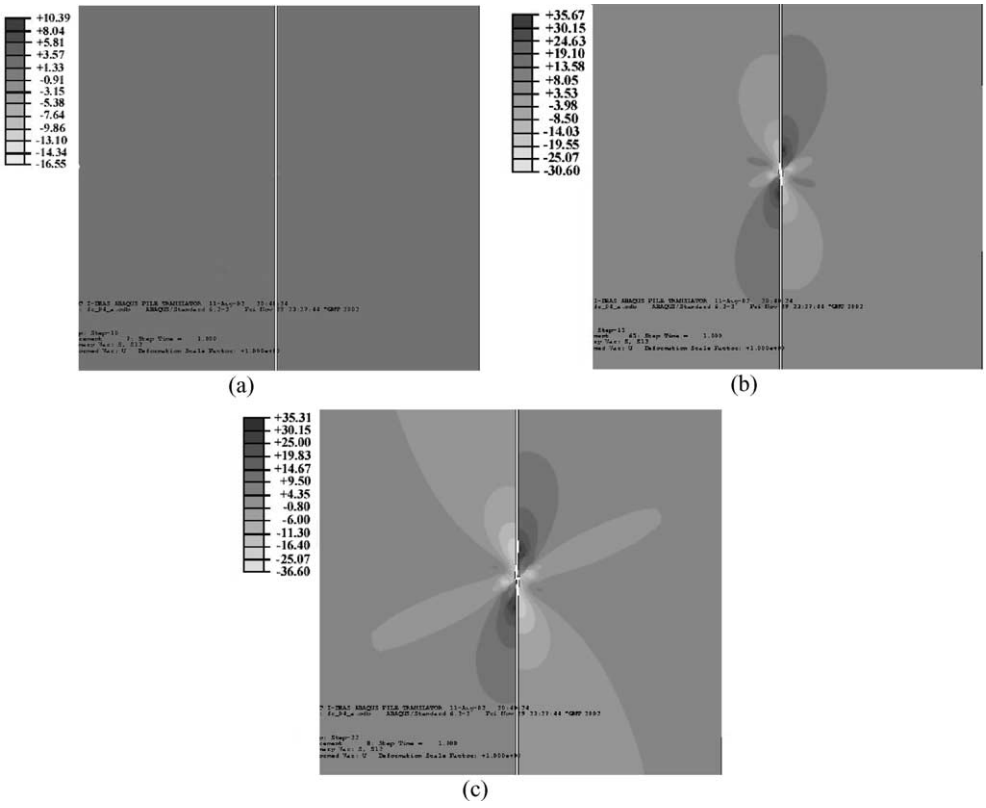

Fig. 6. Shear stress field around the compressive fibre break: (a) applied strain = −0.465% (no fibre break is introduced), (b) applied strain = −0.55% (introduction of the fibre break), and (c) applied strain = −0.7% (all values in MPa). The coefficient of friction between the fibre fragments is 0.4.

can be seen in Fig. 5, which shows the interfacial shear stress (ISS) along the fibre/matrix interface. ISS is zero everywhere, as it should be, except the area near the fibre discontinuity with its absolute higher value being ~ -17 MPa.

Fig. 6 depicts the shear stress contours (σ_{12}) around the fibre break at three different applied strains, (a) $\varepsilon_{11} = -0.465\%$ (the fibre break is not yet introduced), (b) $\varepsilon_{11} = -0.55\%$ (fibre break introduction), and (c) $\varepsilon_{11} = -0.70\%$. It can be easily seen that the shear stress perturbation due to the initial geometrical imperfection (Fig. 6(a)) is much lower than the perturbation created by the fibre break (Fig. 6(b) and (c)). Thus, it can be safely assumed that the initial fibre imperfection has minor effect on the overall analysis, although the stress values are influenced exactly at the fibre break location and for this reason stress values at these points will not be considered in the analysis.

3.2. Effect of friction between the fibre fragments

Fig. 7 shows the FEA predictions of the axial fibre stress profile in the vicinity of a compressive fibre break. It can be seen that for a coefficient of friction of 0.4 the numerical data agrees relatively well with the experimental values, except at $x \cong 0$ due to the model definition as it was explained in the previous section. An important observation is that in contrast to the tensile case (Van den Heuvel et al., 1998; Nath et al., 1996), the fibre stress profile is quite asymmetric around the fibre break. This is due to the fibre bending as the fibre fragments slide past each other after the onset of fibre failure. These results also suggests that one-dimensional analyses such as shear-lag models would fail to accurately capture the mechanics of the problem as it is clear that this fibre failure mode causes also geometrical non-linearities. Fig. 8 depicts another set of experimental data of the same fibre and applied strain ($\varepsilon_{11} = -0.55\%$) but at different position along the fibre length. It can be observed that in this case a higher coefficient of friction between the fibre fragments is needed in order to match the experimental values. At this point some reasons to explain the mismatch between numerical and experimental values should be mentioned. Except the model's imperfection at the fibre break location, the experimental data presents themselves a high level of noise since a very detailed mapping of the fibre stress was attempted (data sampling every 2 μm near the fibre fracture (Goutianos et al., 2002a)). Moreover, during data acquisition some parts of the fibre were invisible to the laser light due to fibre overlapping as the fibre fragments slide past each other (see Fig. 1(a)). Furthermore, the laser spot was of about 2 μm, whereas the fibre diameter is 6.6 μm and it was impossible to control the

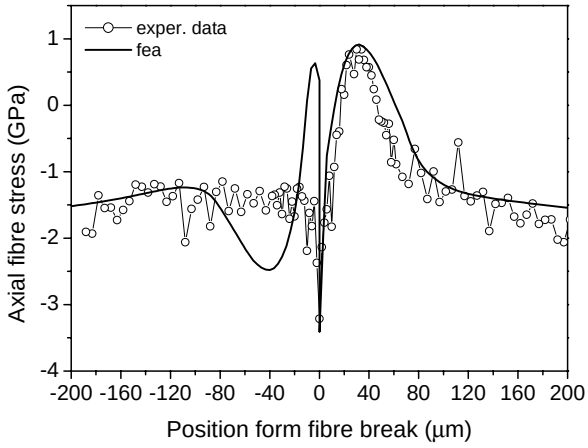

Fig. 7. Axial fibre stress (σ_{11}) in the vicinity of a compressive fibre break ($x = 0$ μm). The applied strain is −0.55%, and the coefficient of friction between the fibre fragments is 0.4.

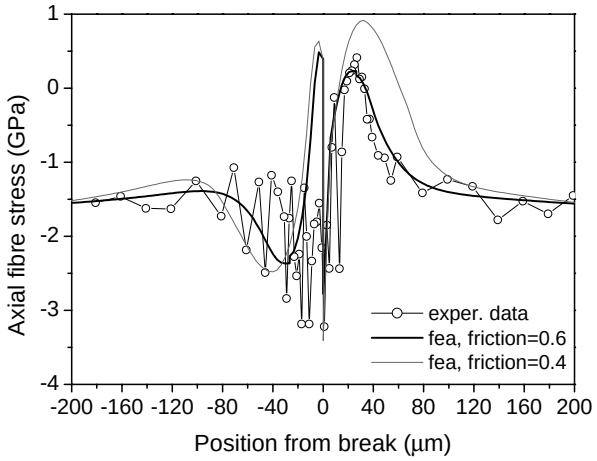

Fig. 8. Axial fibre stress (σ_{11}) in the vicinity of a compressive fibre break ($x = 0$ μm). The applied strain is −0.55%, and the coefficient of friction between the fibre fragments is 0.4 and 0.6, respectively.

point of the fibre fragment where the laser light was focused–as it will be shown later the fibre stress significantly varies across its section near the fibre break position. Finally, as mentioned above the angle between the fibre fragments was set to 45° in the model definition. However, in reality it is expected that more probably there might be small deviations from this value, which would change the effective coefficient of friction between the fibre fragments as a result of the change of the normal force component in the plane of fracture. Considering the above, it can be argued that model's predictions agree well with the experimental findings.

The different coefficient of friction between the fibre fragments used in Figs. 7 and 8 could be explained by the problems during data sampling previously mentioned. However, it might be possible that fibre breaks in the same fibre can have different values of coefficient of friction. This is also supported by the experimental data reported by Goutianos et al. (2002a), where large differences between types of breaks in the same fibre were observed, which cannot be explained by the experimental error of the technique used.

3.3. Stress field in the vicinity of a compressive fibre break

In this section the stress field around a compressive fibre break will be investigated. As it was mentioned above this problem concerning the axial fibre stress was already experimentally investigated by Goutianos et al. (2002a). However, as it is mentioned the derivation of the ISS, in the vicinity of a compressive fibre break, from the fibre stress is not accurate since the balance of forces argument, used successfully in similar problems in tension, is not valid. Thus here, after having validated the model so far by comparing the axial fibre stress obtained from the finite element analysis with the experimental data, the interfacial shear and transverse stresses will be derived.

Fig. 9 depicts the axial fibre stress along the fibre length (the fibre break position is at $x = 1000$ μm) at three different applied strains, −0.55% (fibre break introduction), −0.6%, and −0.7%, respectively. It can be easily seen that the compressive ineffective length is of the order of ∼100 μm, much smaller when compared to the tensile ineffective length (∼500 μm). This can be explained by the fact that the fibre fragments remain in contact after fracture and thus stresses can still be transmitted between the fibre fragments. Another important observation is that the fibre stress profile does not change drastically after fracture with increasing applied strain, which is in agreement with the experimental data reported by Goutianos et al.

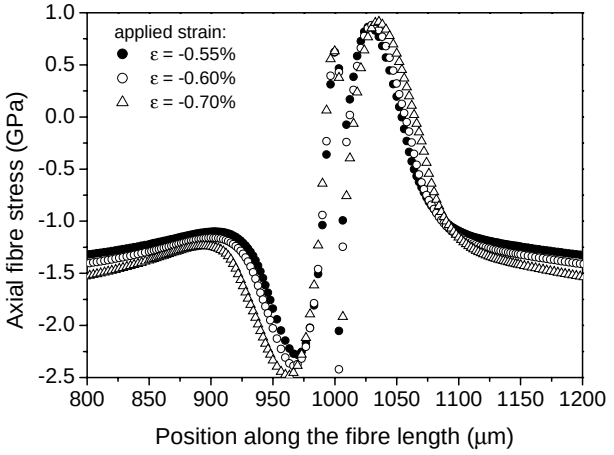

Fig. 9. Axial fibre stress (σ_{11}) in the vicinity of a compressive fibre break ($x = 1000$ μm) at different applied strains (ε_{11}), −0.55%, −0.60%, and −0.70% respectively. The coefficient of friction between the fibre fragments is 0.4.

(2002a). Finally, the far-field stress values (far from the fibre break location) are much lower than predicted by applying Hooke's law, i.e. for $\varepsilon_{11} = -0.55\%$, σ_{11} should be around −2.1 GPa, whereas from Fig. 9 σ_{11} is only 1.25 GPa. The fibre fragments behave like a column that cannot sufficiently support the applied load. Due to the relative movement between the fibre fragments, the load applied to the fibre is partially dissipated to the matrix material. This is in distinct contrast with what is observed in the case of tensile loading, where the far-field fibre stress (or strain) is always equal to the applied stress (or strain) unless the fibre fragment length is less than the critical fibre length or excessive yielding and debonding takes place at strain exceeding quite enough the failure strain of the fibres.

Concerning the interfacial shear stresses from Fig. 10 it can be observed that similar to the axial fibre stress ISS almost barely changes with increasing applied strain. The same can also be seen in Fig. 6(b) and (c), where the shear stresses mainly change in the direction transverse to the fibre through the matrix material. Furthermore, the ISS profile is quite different between the side of the fibre which is under compression (maximum ISS $\sim$ 22 MPa) and the side which is under tension (maximum ISS $\sim$ 30 MPa).

Fig. 11 shows the transverse stresses at the fibre/matrix interface. The analysis of these stresses in the case of tensile fibre fragmentation tests is usually ignored since they are compressive and thus do not lead to transverse cracking. In the case of compressive fragmentation, however, these stresses are positive (tensile) and hence if they exceed the matrix failure stress (under the assumption that the interfacial strength is equal to the matrix strength) failure will occur. From Fig. 11, ignoring the high values near the fibre break location (at $x = 1000$ μm), we can conclude that transverse stresses do not cause transverse interfacial failure for this material system within the applicability of the current model used.

From the above results some distinct differences between the compressive and tensile fragmentation process (Nath et al., 1996; Van den Heuvel et al., 1998) can be immediately identified. As it was mentioned above, the ineffective length in compression is extremely small compared to that one in tension. Moreover, as it was shown, the stress profiles (σ_{11}^{f}, σ_{22}^{m}, and σ_{12}^{m}) do not drastically change in the fibre direction with increasing the applied strain after the event of fibre fracture. On the other hand, from Fig. 6 (shear stresses) it can be seen that this is not the case in the direction transverse to the fibre axis. This is even more clear if the transverse stresses are considered. Fig. 12 depicts the transverse stress contours at an applied strain level of −0.55%. It can be easily seen that the main change in the stress field is in the transverse direction. Hence, it can be assumed that a compressive shear fibre break results in a very local stress perturbation field and the associated damage propagates in the transverse direction rather than in the longitudinal direction.

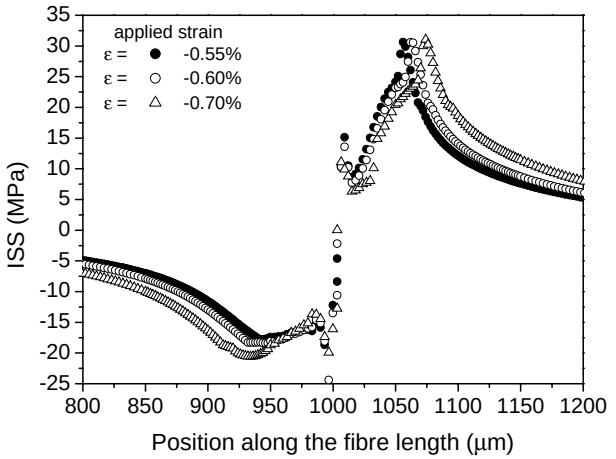

Fig. 10. Interfacial shear stress (σ_{12}) in the vicinity of a compressive fibre break ($x = 1000$ μm) at different applied strains (ε_{11}) −0.55%, −0.60%, and −0.70% respectively. The coefficient of friction between the fibre fragments is 0.4.

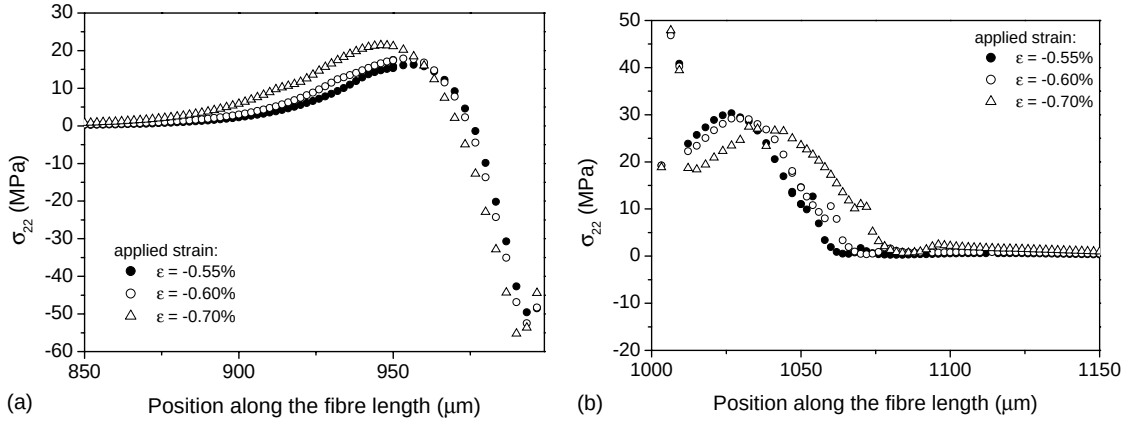

Fig. 11. Transverse stress (σ_{22}) at the fibre matrix interface at different applied strains (ε_{11}), −0.55%, −0.60%, and −0.70% respectively. The coefficient of friction between the fibre fragments is 0.4. Transverse stresses at (a) the left side and (b) the right side of the fibre break.

Additionally as it was shown by Boll et al. (1990), and experimentally supported by our previous work (Goutianos et al., 2002a), that compressive failure of the fibres is not governed by fibre flaws. These suggestions are in agreement with the results of Nakatani et al. (1999) who investigated in detail the distribution of the compressive and tensile strength of carbon fibres. They found that the fibre length dependence of the average fibre compressive strength is much smaller than those of the tensile strength. More importantly, they reported significantly larger value of the shape parameter of the Weibull distribution for the carbon fibre compressive strength ($\beta = 32$) than the fibre tensile strength ($\beta = 6.1$). Based on these results, they also suggested that the scattering of the fibre tensile strength comes from the stochastic nature of the existence and severity of defects and irregularities on the fibre structure. On the other hand, the fibre compressive strength, according to the same authors, depends mainly on intrinsic material properties of the fibre. This observation in conjunction with the current findings that the stress field, around a compressive

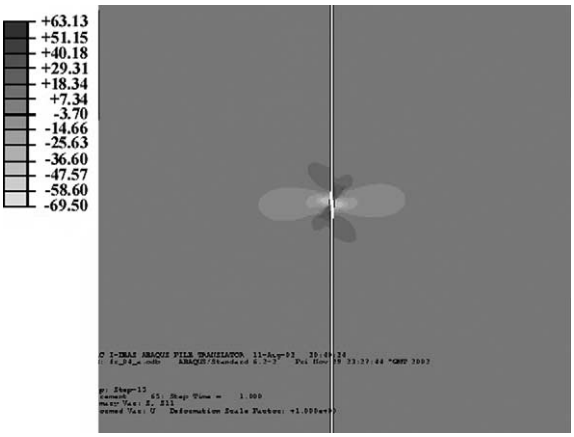

Fig. 12. Transverse stress contours around the compressive fibre break at an applied strain of −0.55% (introduction of the fibre break). The coefficient of friction between the fibre fragments is 0.4 (all values in MPa).

fibre break, changes at a higher rate in the transverse direction could explain the sudden catastrophic failure observed in full unidirectional composites tested in compression. That is, an initial fibre fracture caused by a stress raiser such as a hole, cut-out or fibre misalignment results in an intense stress perturbation in the transverse direction, and as soon as the stress in the nearest adjacent fibre reaches it's failure strength this fibre will instantaneously break at this point (which is normally at a certain small angle with the initial fibre failure as can be seen in Fig. 6(c)) since the failure pattern cannot be deflected by the existence of fibre flaws as it happens in the case of tensile loading as suggested above. As soon as more fibres fail then catastrophic failure takes place at a well defined plane, which lies at an angle different from 90° to the load direction as also shown by Garland et al. (2001). This localised damage zone could then easily cause a local instability leading to kink band formation. This proposed failure mechanism could explain the typical compressive failure modes shown in Fig. 1(b) and (c).

3.4. Effect of matrix modulus

It is well known that the tensile properties of fibrous composites have been significantly improved over the past decades by improving the fibre properties, understanding the role of the interface and optimising the fibre/matrix adhesion, as well as matrix material. However, this is not the case concerning the compressive properties where not much improvement was achieved. In the following sections a parametric analysis of the matrix properties on the stress field generated by a compressive fibre break is performed with the final aim to improve the compressive strength by using a matrix with the appropriate properties. The matrix behaviour is now modelled as elastic–perfectly plastic material. First, the effect of the matrix Young's modulus will be addressed. A variation of the matrix Young's modulus can be seen also as a variation of its shear modulus.

Fig. 13 shows the axial fibre stress profiles along the fibre length for three different matrix moduli of 1.5, 2.0, and 2.5 GPa, respectively. The matrix yield stress is 45 MPa in all the cases. It can be observed that the stiffer the matrix the lesser the fibre fragments can bend and therefore lower maximum fibre tensile and compressive stresses can be attained. On the other hand, the far-field fibre stress is higher for a stiffer matrix.

Concerning the ISS profiles it can be observed from Fig. 14 that for the side of the fibre fragment which is under tension (Fig. 14(b)) all three cases examined show very similar behaviour (maximum ISS = 22 MPa).

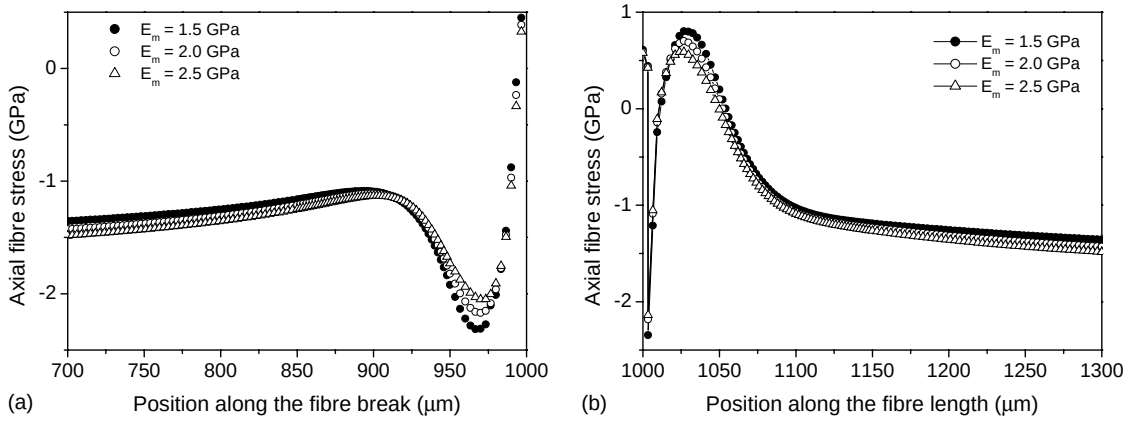

Fig. 13. Axial fibre stress (σ_{11}) in the vicinity of a compressive fibre break ($x = 1000$ μm) for three different matrix modulus, 1.5, 2, and 2.5 GPa respectively. The coefficient of friction between the fibre fragments is 0.4 and the applied strain is −0.55%.

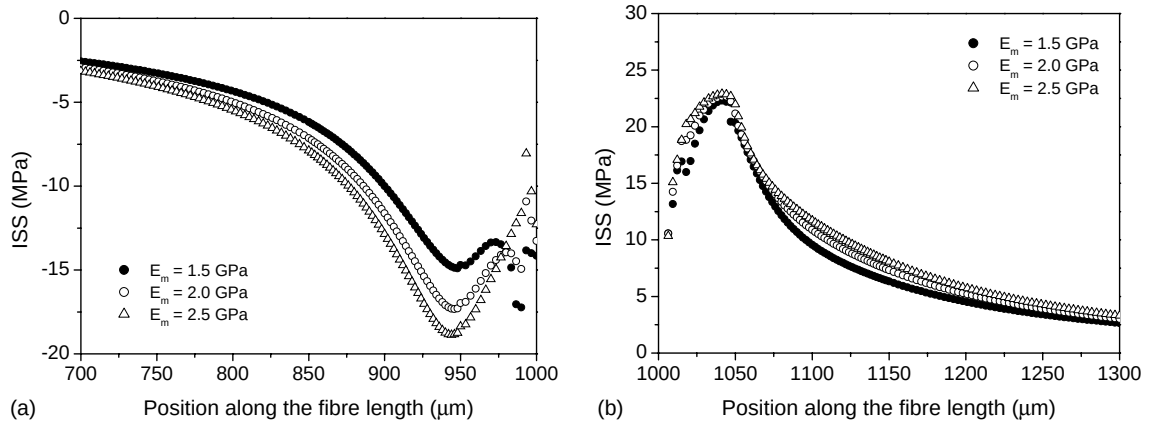

Fig. 14. Interfacial shear stress (σ_{12}) in the vicinity of a compressive fibre break ($x = 1000$ μm) for three different matrix modulus, 1.5, 2, and 2.5 GPa respectively. The coefficient of friction between the fibre fragments is 0.4 and the applied strain is −0.55%.

In the case of a matrix with a lower modulus of elasticity the stress build-up from the fibre break is slightly lower. However, at the compressive side of the fibre (Fig. 14(a)) the effect of the different matrix moduli is more pronounced. A high matrix Young's modulus results in much higher shear stresses. For $E_m = 2.5$ GPa the maximum ISS is ~20 MPa, whereas for $E_m = 1.5$ GPa the maximum ISS is only ~15 MPa.

The transverse stresses are investigated in Fig. 15. Fig. 15(a) depicts the transverse stresses in the side of the fibre fragment, which is under compression and Fig. 15(b) the side, which is under tension. It can be seen from Fig. 15(a) that the higher transverse stresses are observed for the stiffer matrix similar to the case of the interfacial shear stresses. Concerning the side, which is under tension, again not much difference between the three different matrix moduli can be observed. In all the cases the maximum attained values are the same, while as the matrix modulus decreases (read: the fibre can bend more easily) σ_{22} decreases at lower rate at a small distance from the fibre break and then rapidly drops to zero.

From the results presented above it can be concluded that a low matrix Young's modulus (or shear modulus) results in larger deformations of the fibre fragments after fibre fracture simply because the matrix

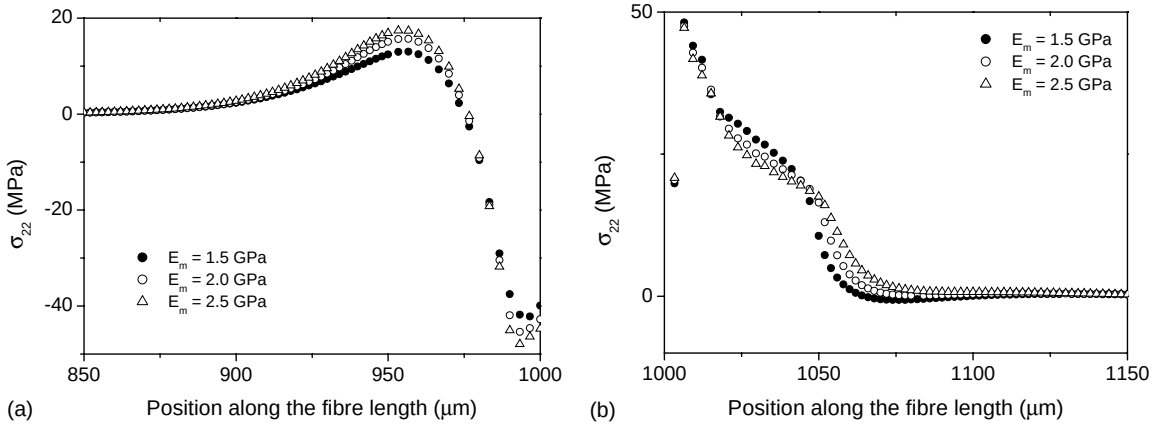

Fig. 15. Transverse stress (σ_{22}) in the vicinity of a compressive fibre break ($x = 1000$ μm) for three different matrix modulus, 1.5, 2, and 2.5 GPa respectively. The coefficient of friction between the fibre fragments is 0.4 and the applied strain is −0.55%.

provides less support to the fibre fragments. In general, however, it can be assumed that a variation in the Young's modulus of the matrix does not drastically alter the stress field caused by the fibre fracture. Additionally, the matrix shear stress patterns in the transverse direction to the fibre break were almost identical for the three different matrix moduli examined. At this point it should be mentioned that Rosen's analysis (Rosen, 1965) treats the problem of compression as a buckling process in an elastic foundation and its predictions are much higher compared with experimental values. From the results of this section, it can be argued that the matrix modulus within the range examined has no direct effect on the compressive fragmentation process.

3.5. Effect of matrix yield stress

In this section the effect of the matrix yield stress will be investigated. For this reason the matrix Young's modulus is kept constant and equal to 2 GPa. Fig. 16 shows the axial fibre stress in the case of three

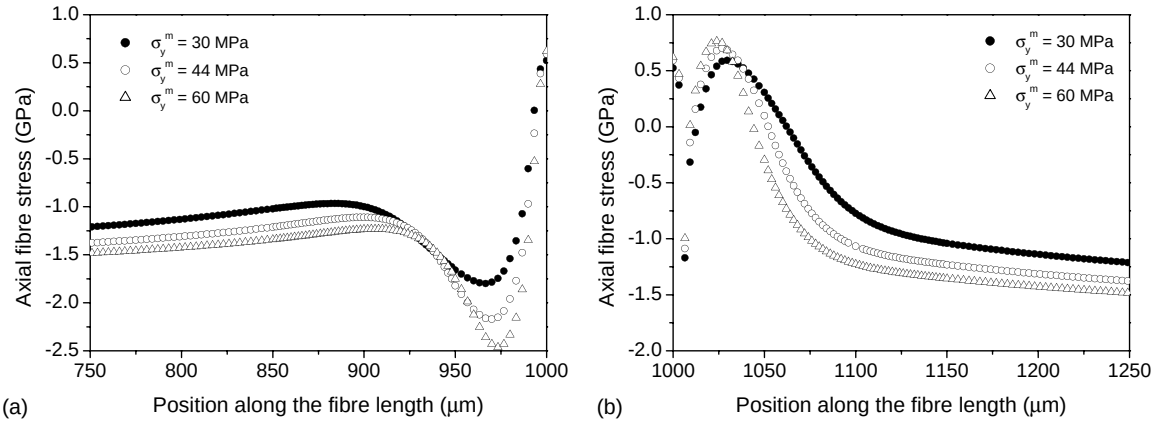

Fig. 16. Axial fibre stress (σ_{11}) in the vicinity of a compressive fibre break ($x = 1000$ μm) for three different matrix yield stresses, 30, 45, and 60 MPa, respectively. The coefficient of friction between the fibre fragments is 0.4 and the applied strain is −0.55%, and the matrix modulus is 2.0 GPa.

different matrix yield stresses 30, 45, and 60 MPa, respectively. It can be easily observed that a low matrix yield stress results in lower maximum fibre stress values and higher ineffective length. Additionally, it is interesting to observe that the effect of the matrix yield stress is more pronounced of the compressive side of the fibre fragment.

The corresponding interfacial shear stresses are plotted in Fig. 17, where it can be seen that the shear stresses are strongly affected by changing the matrix yield stress. Moreover, excessive yielding occurs for a low matrix yield stress (see Fig. 17(b), whereas no yielding can be identified at the compressive side of the fibre (Fig. 17(a)).

The transverse stresses for the three different matrix yield stresses used are given in Fig. 18(a) (compressive side of the fibre fragment) and Fig. 18(b) (tensile side of the fibre fragment). In both cases a low

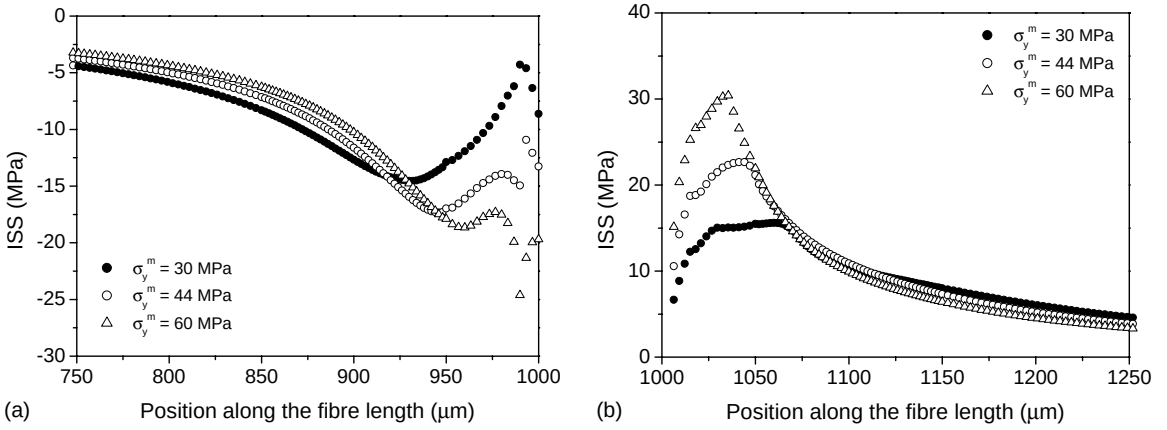

Fig. 17. Interfacial shear stress (σ_{12}) in the vicinity of a compressive fibre break ($x = 1000$ μm) for three different matrix yield stresses, 30, 45, and 60 MPa, respectively. The coefficient of friction between the fibre fragments is 0.4 and the applied strain is −0.55%, and the matrix modulus is 2.0 GPa.

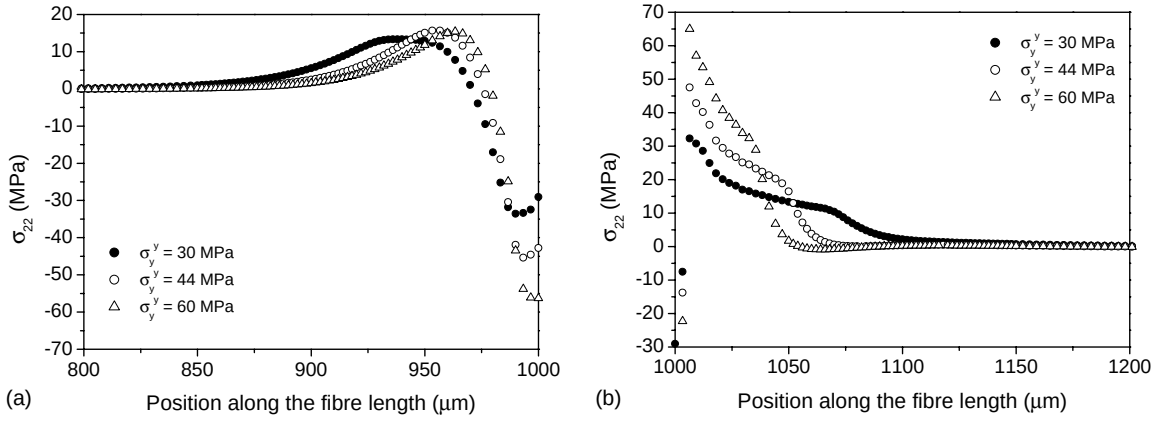

Fig. 18. Transverse stress (σ_{22}) in the vicinity of a compressive fibre break ($x = 1000$ μm) for three different matrix yield stresses, 30, 45, and 60 MPa, respectively. The coefficient of friction between the fibre fragments is 0.4 and the applied strain is −0.55%, and the matrix modulus is 2.0 GPa.

matrix yield stress results in a higher affected zone caused by the fibre break as the matrix is more compliant and therefore the fibre fragments can bend more easily. The difference between the different matrix yield stresses chosen are now more clear in the side of the fibre fragment which is under tensile loading.

It is clear from the results presented that the matrix yield is a key parameter in studying the compressive behaviour of composites. A high matrix yield stress is essential in order to improve the compressive properties of fibrous composites. This is in agreement with the results of i.e. Argon (1972), Budiansky (1983), and Fleck et al. (1995), the only basic difference with their analysis is that the primary damage mechanism is the fibre fragmentation itself.

Next a comparison between an elastic ($\sigma_y^m = 0$) and elastic–perfectly plastic matrix ($\sigma_y^m = 45$ MPa) will be performed to highlight the effect of matrix non-linearity. Fig. 19 depicts the axial fibre stress profiles

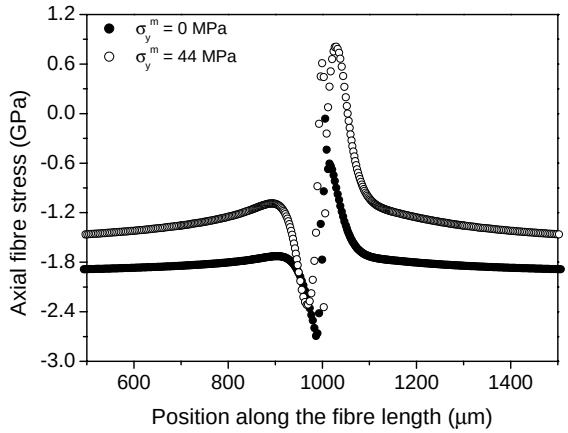

Fig. 19. Axial fibre stress (σ_{11}) in the vicinity of a compressive fibre break ($x = 1000$ μm) for (a) an elastic matrix and (b) an elastic–perfectly plastic matrix ($\sigma_y^m = 45$ MPa). The coefficient of friction between the fibre fragments is 0.4 and the applied strain is −0.55%, and the matrix modulus is 1.5 GPa.

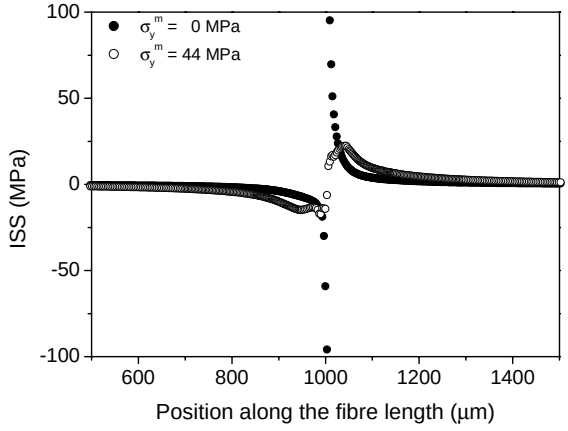

Fig. 20. Interfacial shear stress (σ_{12}) in the vicinity of a compressive fibre break ($x = 1000$ μm) for (a) an elastic matrix and (b) an elastic–perfectly plastic matrix ($\sigma_y^m = 45$ MPa). The coefficient of friction between the fibre fragments is 0.4 and the applied strain is −0.55%, and the matrix modulus is 1.5 GPa.

along the fibre length (fibre break location at $x = 1000$ μm) for the two different matrices. The ineffective length does not show large differences although it is lower for the elastic matrix. The most striking observation is that for the elastic matrix the stress profile is shifted downwards to higher compressive values, i.e. the far-field axial fibre stress is −1.9 MPa, whereas for the elastic–perfectly plastic matrix is only −1.5 MPa. Concerning the ISS profiles it can be seen from Fig. 20 that the elastic interfacial shear stresses are unacceptably high (100 MPa) exceeding the shear yield stress of any commercial epoxy matrix. In the elastic case the matrix is so stiff that the fibre fragments display small lateral deformations and as a consequence the perturbation of shear stresses around the fibre break is minor. On the other hand, if the numerical predictions for the elastic matrix concerning the axial fibre stress are compared with the experimental data presented in Figs. 7 and 8, then it can be observed that plasticity needs to be taken into account in order to model the compressive behaviour of fibrous composites.

4. Conclusions

A numerical investigation of the compressive behaviour of high-modulus carbon fibres embedded in an epoxy matrix was performed. First the FE model was validated by comparing numerical predictions with experimental data. It was shown that:

1. The stress build-up emanating from a compressive fibre break is quite different from that in tension. In contrast to the tensile case in compression the fibre stress at a fibre break does not necessarily drop to zero.
2. The rate of stress transfer from a compressive fibre break is extremely high, since load transmission occurs between the fibre fragments, and therefore the corresponding ineffective length is extremely small.
3. The matrix modulus of glassy polymers has no drastic effects on the stresses generated by the fibre fracture and thus enhancement of the compressive strength cannot be achieved by increasing the matrix modulus (for an elasto-plastic matrix).
4. Matrix plasticity is a key parameter in modelling the compressive behaviour of composites–a high yield stress is required for compressive strength improvement.

References

Amer, M.S., Schadler, L.S., 1997. Stress concentration phenomenon in graphite/epoxy composites: tension/compression effects. Compos. Sci. Technol. 57, 1129–1137.

Argon, A.S., 1972. Fracture of composites. In: Treatise of Material Science and Technology, vol. 1. Academic Press, New York, NY.

Boll, D.J., Jensen, R.M., Cordner, L., 1990. Compression behavior of single carbon filaments in an epoxy matrix. J. Compos. Mater. 24, 208–219.

Budiansky, B., 1983. Micromech. Comput. Struct. 16 (1–4), 3–12.

Budiansky, B., Fleck, N.A., 1991. Compressive failure of fibre composites. J. Mech. Phys. Solids 41 (1), 183–211.

Byskov, E., Christoffersen, J., Christensen, C.D., Poulsen, J.S., 2002. Kinkband formation in wood and fiber composites—Morphology and analysis. Int. J. Solids Struct. 39, 3649–3673.

Christensen, R.M., De Teresa, S.J., 1997. The kink band mechanism for the compressive failure of fiber composites. J. Appl. Mech. 64, 1–6.

Fleck, N.A., Deng, L., Budiansky, B., 1995. Prediction of kink width in compressed fiber composites. J. Appl. Mech. 62, 329–337.

Garland, B.D., Beyerlein, I.J., Schadler, L.S., 2001. The development of compression damage zones in fibrous composites. Compos. Sci. Technol. 61, 2461–2480.

Goutianos, S., Peijs, T., Galiotis, C., 2002a. Mechanisms of stress transfer and interface integrity in carbon/epoxy composites under compression loading. Part I: Experimental investigation. Int. J. Solids Struct. 39, 3217–3231.

Goutianos, S., Galiotis, C., Peijs, T., 2002b. Monitoring the fibre compressive strain distribution in simple model composite geometries. In: Sol, H., Degrieck, J. (Eds.), Proceedings of the 10th European Conference on Composite Materials (ECCM-10)—Composites for the future, Brugge, Belgium, June 3–7, 2002, paper 286, pp. 1–8.

Hsu, S.-Y., Vogler, T.J., Kyriakides, S., 1999a. Inelastic behavior of an AS4/PEEK composite under combined transverse compression and shear. Part II: Analysis. Int. J. Plast. 15, 807–836.

Hsu, S.-Y., Vogler, T.J., Kyriakides, S., 1999b. On the axial propagation of kink bands in fiber composites. Part II: Analysis. Int. J. Solids Struct. 36, 575–595.

Jensen, H.M., 2002. Residual stress effects on the compressive strength of unidirectional fibre composites. Int. J. Solids Struct. 50, 2895–2904.

Kozey, V.V., 1993. Splitting-related kinking failure mode in unidirectional composites under compressive loading. J. Mater. Sci. Lett. 12, 43–47.

Lankford, J., 1995. Compressive failure of fibre-reinforced composites: Buckling, kinking, and the role of the interface. J. Mater. Sci. 30, 4343–4348.

Lesko, J.J., Swain, R.E., Cartwright, J.M., Chin, J.W., Reifsnider, K.L., 1994. Interphases developed from fiber sizings and their chemical–structural relationship to composite compressive performance. J. Adhes. 45, 43–57.

Madhukar, M.S., Drzal, L.T., 1992. Fiber-matrix adhesion and its effects on compressive mechanical properties. III. Longitudinal (0°) compressive properties of graphite/epoxy composites. J. Compos. Mater. 26 (3), 310–333.

Nakatani, M., Shioya, M., Yamashita, J., 1999. Axial compressive fracture of carbon fibres. Carbon 37, 601–608.

Narayanan, S., Schadler, L.S., 1999a. Mechanisms of kink-band formation in graphite/epoxy composites: A micromechanical experimental study. Compos. Sci. Technol. 59, 2201–2213.

Narayanan, S., Schadler, L.S., 1999b. Assessment of strains along fiber surface features in graphite/epoxy composites loaded in compression. Compos. Sci. Technol. 59, 1589–1596.

Nath, R.B., Fenner, D.N., Galiotis, C., 1996. Elasto-plastic finite element modelling of interfacial failure in model Kevlar-49 fibre–epoxy composites. Composites Part A 27, 821–832.

Rosen, B.W., 1965. Mechanism of composite strengthening. In: Fibre Composite Materials. American Society of Metals, Metals Park, OH, pp. 37–75.

Sastry, A.M., Phoenix, S.L., 1993. Load distribution near non-aligned fibre breaks in a two dimensional unidirectional composite using break-influence superposition. J. Mater. Sci. Lett. 12, 1596–1599.

Schapery, R.A., 1995. Prediction of compressive strength and kink bands in composites using a work potential. Int. J. Solids Struct. 32, 739–765.

Sirivedin, S., Fenner, D.N., Nath, R.B., Galiotis, C., 2000. Matrix crack propagation criteria for model short-carbon fibre/epoxy composites. Compos. Sci. Technol. 60, 2835–2847.

Soutis, C., Curtis, P.T., 2000. A method for predicting the fracture toughness of CFRP laminates failing by fibre microbuckling. Composites Part A 31, 733–740.

Soutis, C., Smith, F.C., Matthews, F.L., 2000. Predicting the compressive engineering performance of carbon fibre-reinforced plastics. Composites Part A 31, 531–536.

Van den Heuvel, P.W.J., Wubbolts, M.K., Young, R.J., Peijs, T., 1998. Failure phenomena in two-dimensional multi-fibre composites: 5. A finite element study. Composites Part A 29, 1121–1135.

Vogler, T.J., Hsu, S.-Y., Kyriakides, S., 2001. On the initiation and growth of kink bands in fiber composites. Part II: Analysis. Int. J. Solids Struct. 38, 2653–2682.